PLANETARY SCIENCE

A potential mantle origin for precursor rocks of high-Mg impact glass beads in Chang'e-5 soil

Chen-Long Ding[1], Alexander Nemchin[2]†, Tim Johnson[2]†, Marc D. Norman[3]†, Yue Guan[1]‡, Lan-Lan Tian[1]‡, Wen-Li Xie[1], Lin-Sen Li[1], Sheng-Di Zhou[1], Ke-Xin Xu[1], Xiao-Lei Wang[1]*

The chemical compositions of most lunar impact glass beads reflect mixing of crustal components including mare basalts, highlands rocks, and KREEP [from high concentrations of K, REE (rare earth element), and P]. However, a few glass beads in the soil from the Chang'e-5 mission have unusually high MgO contents that require distinct target compositions. The young age of these high-MgO glass beads suggests an origin through impact melting of ultramafic target rocks with abundant pyroxene and olivine. While such targets might represent cumulates of mare basalts, impact melts, or Mg-suite rocks, they appear unlike any sampled lunar lithologies. Alternatively, these high-Mg beads might be sampling the upper mantle brought to the surface by the Imbrium basin–forming event.

INTRODUCTION

All lunar soils contain glass beads of volcanic and impact origin (*1–6*). Lava fire fountain eruptions produce volcanic beads, whereas impact glasses form when asteroids hitting the Moon vaporize or melt surface materials. Collectively, they provide a record of magmatic processes and compositional variations of the lunar mantle (*7–11*), potential water reservoirs on the Moon (*12–14*), and the impact history of the Moon and inner Solar System (*15–17*). Soils collected at Apollo landing sites proximal to extensive basaltic terranes have high proportions of volcanic glasses, whereas impact glasses dominate soils collected within highland regions (*5, 18, 19*). The Chang'e-5 mission retrieved soil that is notably different. Although this landing site is within a large field of basalt, some 150 to 200 km from the nearest highland region, impacts into this basalt and the overlying regolith produced most glass beads in the soil rather than volcanic eruptions (*11, 13, 14, 16*). However, several compositionally distinct groups of beads representing a few percent of the population probably originated from impacts into terranes outside of the Chang'e-5 basalt unit (*11, 16*). Of particular interest here is a group of glasses with MgO contents exceeding 18 wt %. Previous study reported seven of these high-MgO glass beads, which correspond to about 4% of the total glass bead population in the Chang'e-5 sample (*16*). The high MgO concentrations clearly differentiate them from the local basalt and regolith at the Chang'e-5 landing site, which have MgO contents ~6.5 wt % (*20*).

Here, we present a detailed chronological and geochemical study of a large (>300 μm) impact bead with a high MgO content comparable to those described previously (*16*). These data provide insights into the origin of other high-MgO impact glass beads recovered from the Chang'e-5 soil.

[1]State Key Laboratory of Critical Earth Material Cycling and Mineral Deposits, Frontiers Science Center for Critical Earth Material Cycling, School of Earth Sciences and Engineering, Nanjing University, Nanjing 210023, China. [2]School of Earth and Planetary Sciences, Curtin University, Perth, WA 6845, Australia. [3]Research School of Earth Sciences, The Australian National University, Canberra, ACT 2601, Australia.
*Corresponding author. Email: wxl@nju.edu.cn
†These authors contributed equally to this work.
‡These authors contributed equally to this work.

RESULTS

We extracted the studied bead from soil split CE5C0600YJFM00501, allocated by the China National Space Administration (CNSA). The bead is green in color and has a curved termination on one side, identifying it as part of a larger broken spherule (Fig. 1). Backscattered electron imaging revealed finely crystalline areas with radiating, elongate, skeletal crystals, which we interpret as the more slowly cooled interior of the original melt droplet. These areas grade into a rim of glass, up to 100 μm thick, disrupted by fragmentation of the original bead (Fig. 1).

Replicate major element compositions of glass and finely crystalline regions, measured using an electron microprobe analyzer, are identical within uncertainties (fig. S1 and data S1). The high MgO content (25.3 to 26.2 wt %) clearly distinguishes this bead from the Chang'e-5 basalt unit and the main population of Chang'e-5 regolith beads (Fig. 2) (*11, 16*). The studied bead also has lower TiO_2, Al_2O_3, FeO_t, and CaO (Fig. 2, A to D).

CE5C0600YJFM00501
G1-GB-1

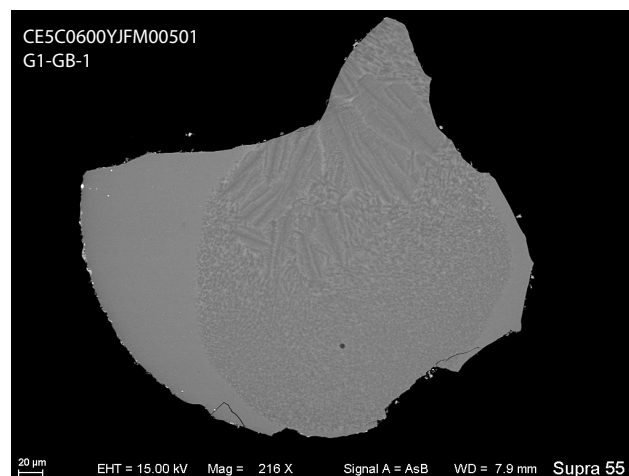20 μm   EHT = 15.00 kV   Mag = 216 X   Signal A = AsB   WD = 7.9 mm   Supra 55

Fig. 1. Microtexture of Chang'e-5 high-MgO glass G1-GB-1 from CE-5C0600YJFM00501. A discontinuous rim of glass up to 100 μm thick surrounds the finely crystalline area, which shows elongated, skeletal crystals in the internal parts of the spherule grading to a microcrystalline texture and homogeneous glass toward the spherule's external surface.
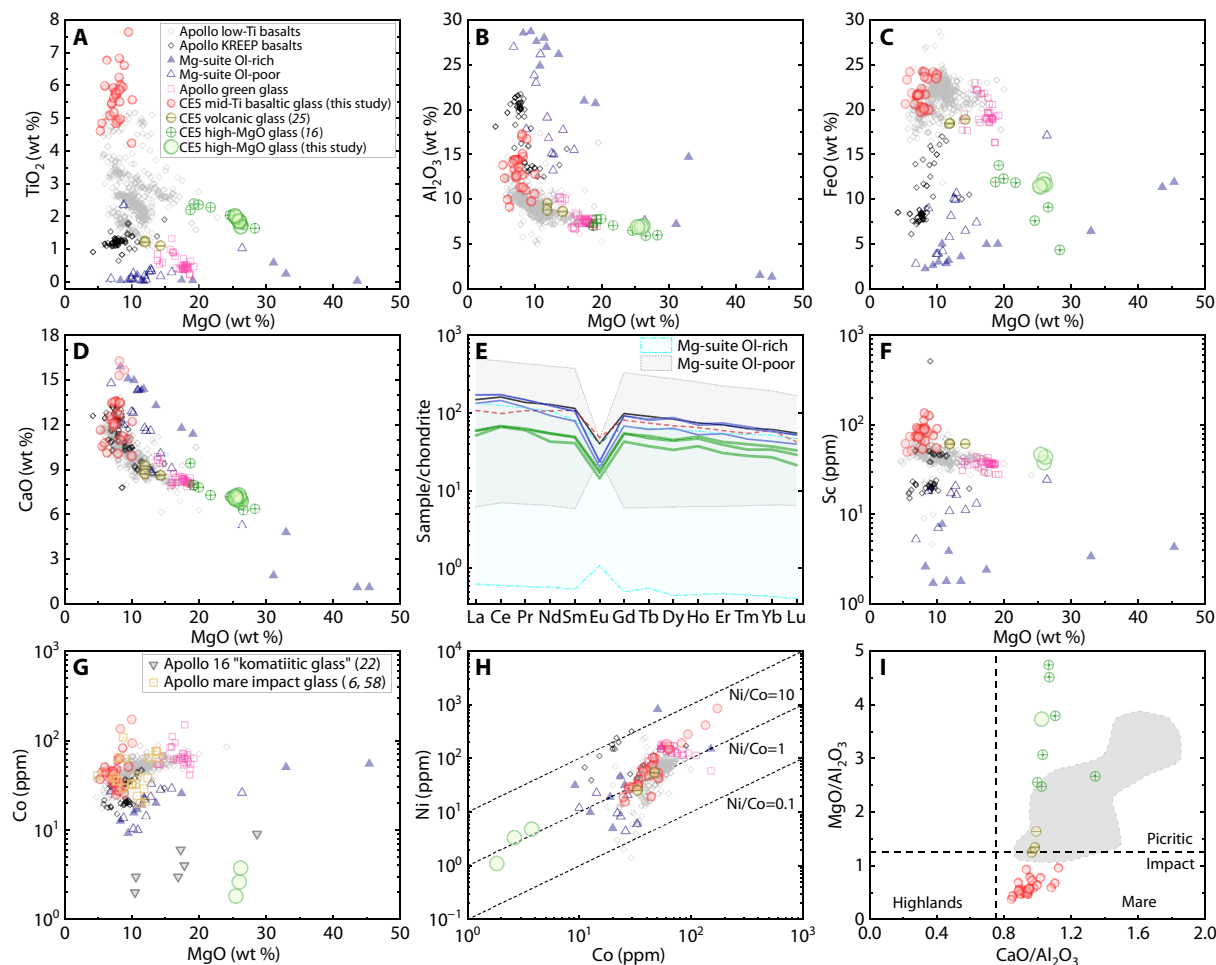
Fig. 2. Chemistry of Chang'e-5 high-MgO glass G1-GB-1. (**A** to **D**) Concentrations of major oxides versus MgO. Compositions of high-MgO glass compared to mid-Ti basaltic beads from the Chang'e-5 sample, the volcanic beads from the Chang'e-5 sample (*25*), Apollo low-titanium basalts, KREEP basalts, Apollo green volcanic glass, and Mg-suite rocks (*30*). The legend in (A) shows symbols representing different rocks and glasses. (**E**) Chondrite-normalized REE patterns from three analyses of the high-MgO glass bead (green solid line). The red pattern (red dashed line) represents an average of mid-Ti basaltic glasses, blue patterns represent three Chang'e-5 analyses of volcanic glasses (*25*), the black pattern represents analysis of the Chang'e-5 soil (*20*), and light cyan and gray fields are Mg-suite rocks (*30*). (**F** to **H**) Some compatible trace elements in high-MgO glass and other lunar materials. Symbols are similar to those used in (A); two additional symbols in (G) show Apollo 16 and 17 mare impact glasses (*6*, *58*) and "komatiitic" glasses (*22*). (**I**) CaO/Al$_2$O$_3$ ratio and MgO/Al$_2$O$_3$ ratio binary diagram distinguishing the volcanic versus impact origin of glass bead in lunar soil samples (*6*). The gray region represents Apollo volcanic glasses (*25*). The published data in all plots are from (*6*, *16*, *22*, *25*, *30*, *58*). The mare basalt database is located at www3.nd.edu/~cneal/Lunar-L/.

Trace element compositions of the glass and finely crystalline portions of the studied bead, measured using secondary ion mass spectrometry (SIMS) (fig. S1), are also within uncertainties, with rare earth element (REE) concentrations ~30 to 50 times higher than chondrite (*21*). Chondrite-normalized patterns show a negative slope (La$_n$/Lu$_n$ = 1.8 to 2.4) and a pronounced negative Eu anomaly (Eu/Eu* = 0.33 to 0.35) (Fig. 2E). Other incompatible elements, such as Zr [168 to 233 parts per million (ppm); fig. S2A] and Th (1.3 to 1.9 ppm; fig. S2B), show similar levels of enrichment relative to chondrite (*21*) but about two times lower than concentrations of these elements in the main group of locally derived glass beads in the Chang'e-5 sample. Although concentrations of Sc (38 to 47 ppm) and V (93 to 119 ppm) resemble those found in the main group of Chang'e-5 glass beads (Fig. 2F and fig. S2C), concentrations of both Ni and Co (1 to 5 and 2 to 4 ppm, respectively) are an order of magnitude

lower than those in the main group of Chang'e-5 beads and almost all other lunar glass beads and rocks (Fig. 2, G and H, and fig. S2D). A notable exception is a small subset of Apollo 16 glass beads described as "komatiitic," which have Co concentrations of 2 to 9 ppm (Fig. 2G) (*22*). The Ni/Co ratios in the analyzed bead (0.6 to 1.3) are much lower than chondritic values (*21*).

Six U–Pb spot analyses of the glass bead by SIMS (fig. S1) define a statistically significant linear fit with a concordia intercept age of 68 ± 10 million years [Ma; MSWD (mean squared weighted deviation), 1.5; probability, 0.13] (Fig. 3) in the three-dimensional ^{204}Pb/^{206}Pb–^{207}Pb/^{206}Pb–^{238}U/^{206}Pb space. The measured ^{207}Pb/^{206}Pb–^{238}U/^{206}Pb compositions fall close to the concordia, indicating no significant addition of meteoritic, lunar, or terrestrial Pb. We interpret the age of 68 ± 10 Ma as the best estimate of the time of formation of the studied bead.
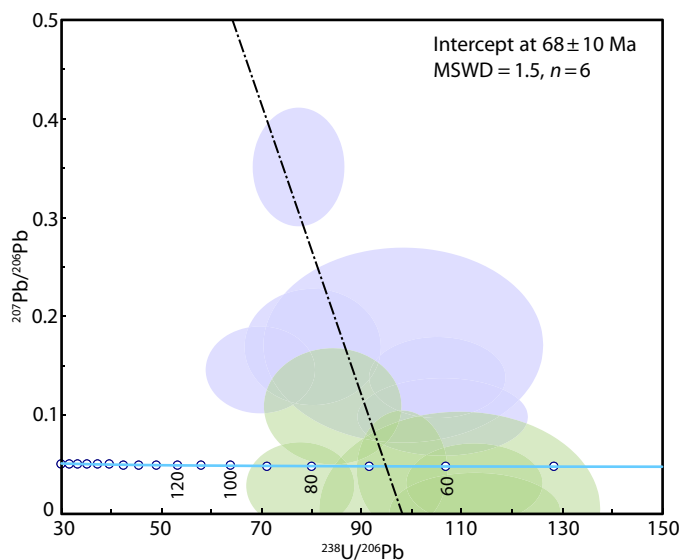
Fig. 3. U–Pb age of Chang'e-5 high-MgO glass G1-GB-1. Tera-Wasserburg U–Pb concordia diagram showing the young age (~68 ± 10 Ma, 2σ) of the glass. Purple error ellipses are uncorrected data, and green error ellipses represent projection of data along the best fit line in the three-dimensional 3D $^{204}Pb/^{206}Pb$–$^{207}Pb/^{206}Pb$–$^{238}U/^{206}Pb$ space.

DISCUSSION

Distinctive characteristics of high-Mg glass beads

Distinguishing a volcanic from impact origin for the high-MgO Chang'e-5 glass beads is critical for their interpretation. Quench textures similar to those preserved in the investigated high-MgO glass bead (Fig. 1) could suggest a volcanic origin (5, 8). However, ultramafic melts are notoriously difficult to quench to a homogeneous glass (23) and the MgO/Al_2O_3 ratio of this bead (~3.7) is higher than those of typical lunar volcanic glasses [less than ~3, e.g., ref. (6)] (Fig. 2I). Notionally, the young age of this bead would imply an impact origin based on the current understanding of lunar volcanism, which is older than 2 billion years, as indicated by the crater size frequency distribution data obtained for the near side of the Moon (24). However, the recent report of three glass beads from the Chang'e-5 regolith with a very young U/Pb age (123 ± 15 Ma), interpreted as volcanic based on their S isotope compositions (25), challenges this perspective. Those glasses are also more magnesian (12 to 14 wt % MgO) than the local basalt and regolith (6.5 wt %) (20) but less magnesian than the high-MgO beads reported earlier (18 to 28 wt % MgO) (16) and here (25 to 26 wt % MgO) (Fig. 2). Sulfur isotopes are not an established petrogenetic indicator for a specific origin of lunar regolith glasses (10) (see also Supplementary Text).

Seven high-MgO Chang'e-5 glass beads, identified previously (16), provide additional evidence supporting an impact origin for the studied high-MgO bead. Three of these beads are homogeneous glasses, while four contain finely crystalline portions surrounded by glass, similar to the bead analyzed here (Fig. 1). These previously described high-MgO beads have ages ranging from 346 ± 47 to 8 ± 3 Ma (16). For all to be of volcanic origin, these beads must represent multiple episodes of volcanism close to the Chang'e-5 landing site during the past 350 million years. However, there is no evidence in the remote sensing data for recent volcanism near the

Chang'e-5 landing site (26). Unlike impact glasses that can be transported over distances of several hundred kilometers, volcanic glasses usually accumulate close to their eruptive centers (26–28). Therefore, while the possibility of very young volcanism on the Moon is provocative, there is no geological evidence for this (26) and we interpret the high-MgO beads in the Chang'e-5 regolith to have an impact origin.

The high-MgO beads are clearly distinct from the main population of Chang'e-5 glass beads and various picritic and impact glasses identified in the Apollo samples, none of which have MgO content exceeding 20 wt % (Figs. 1 and 2I). A few "komatiitic" beads from the Apollo 16 regolith breccias have high MgO contents (22), but only one (65715, 54) has a MgO content (~28 wt %) comparable to the Chang'e-5 high-MgO beads (Fig. 2G). It also has much higher Al_2O_3 (12.5 wt %) and lower FeO (3.1 wt %) (22). Nevertheless, all of the Apollo 16 komatiitic beads are enriched in incompatible trace elements and have low Co concentrations (Ni is not reported) similar to those in the Chang'e-5 high-MgO glasses (Fig. 2G). The low Co contents of these komatiitic beads likely reflect reduction of FeO to metal and separation of metallic and silicate melts during the bead-forming impact (22).

Possible target for the high-Mg glass

The MgO content of the high-MgO Chang'e-5 beads eliminates all known mare and KREEP (from high concentrations of K, REE, and P) basalts, including a clast of high-Mg (~15% MgO), low-Ti basalt recently discovered in a breccia fragment from the Chang'e-5 sample (29), as potential target rocks for the beads (Fig. 2). Similarly, all olivine-poor feldspathic plutonic rocks, such as anorthosites, norites, and gabbronorites, are too enriched in Al and depleted in Mg to be viable sources (Fig. 2). Most rocks of the lunar crustal Mg-suite show distinctly lower TiO_2 content compared to the high-MgO glass beads (30). Rare olivine-rich Mg-suite rocks, such as spinel troctolites and dunites, are chemically closest to the high-MgO glass beads, although the dunites have higher MgO content and lower Al_2O_3 and CaO (30). Lunar troctolites have similar MgO contents but higher Al_2O_3 and CaO and lower FeO (30).

One of the most magnesian mare basalt samples, 12005 (~20 wt % MgO), has a cumulate texture with ~56 vol % pyroxene, ~30 vol % olivine, and ~11 vol % plagioclase (31, 32). Such cumulates may represent the target of the impact that formed high-MgO beads. However, this particular sample has significantly higher FeO (22 versus 12 wt %) and lower SiO_2 (42 versus 47 wt %) compared to the high-MgO beads (32). Another unusual sample from the Apollo 16 site, 67667, classified as a feldspathic lherzolite (33), has higher FeO (17 wt %) and lower SiO_2 (42 wt %) compared to the Chang'e-5 high-MgO beads.

The incompatible trace element concentrations of the studied high-MgO glass bead fall near the middle of the range observed in Mg-suite plutonic rocks (Fig. 2E). This might suggest that Mg-suite rocks could have been a target of the impact event that produced the high-MgO glasses. However, Mg-suite dunites and spinel troctolites with >25 wt % MgO have incompatible element (Zr, Y, REE, and Hf) concentrations significantly lower than those of the bead (Fig. 2 and fig. S2). Both mare basalt sample 12005 and lherzolite sample 67667 also show lower concentrations of incompatible elements. For example, REE concentrations in both samples are three to four times lower than in the high-MgO bead studied here (32, 33). A similar three- to fourfold depletion relative to the high-MgO bead occurs in a recently described Chang'e-5 low-Ti basalt clast (29).

In summary, the major and trace element compositions of known lunar rocks indicate that none are plausible target rocks for the high-MgO beads from the Chang'e-5 soil (*30*). This implies previously unsampled ultramafic (olivine and pyroxene rich and plagioclase poor) rocks near the surface of the Moon. Such ultramafic rocks may represent cumulates from Mg-suite or mare basalt magmas (*32*). Alternatively, the ultramafic source regions required for these Mg-rich glasses may represent exposures of the lunar mantle. Whereas ultramafic crustal cumulates can form at shallow levels in the lunar crust, mantle materials likely require large (potentially basin-forming) events to bring them to the surface (*34, 35*).

Phase equilibrium modeling can constrain the melting behavior, abundance, and composition of minerals of plausible target rocks corresponding to the bulk chemical compositions of the studied high-MgO Chang'e-5 beads under a range of pressure-temperature (*P-T*) conditions (*36*). We calculated a *P-T* diagram for 800° to 1700°C and 0.01 to 4 kbar based on the measured bulk composition of the studied high-MgO glass bead (fig. S3) with the maximum *P* (4 kbar) corresponding to a depth of around 75 km, encompassing the lunar crust and uppermost mantle (*37*). A homogeneous melt with the bulk composition of the studied bead requires a minimum temperature of 1600°C based on the calculated liquidus temperature

(fig. S3, solid red line). During cooling, an equilibrated melt of this composition would have become entirely solid at around 1150°C (solid red line in fig. S3). Calculated mineral proportions do not change internally beyond a few percent across the range of modeled *P-T* conditions and are consistent with previously analyzed high-MgO beads (data S3) (*16*). The average compositions of model precursor rocks determined for all the high-MgO beads fall near the boundary between plagioclase-bearing ultramafic rocks and olivine-gabbro norites (Fig. 4A and data S3). Most are enriched in orthopyroxene relative to clinopyroxene and olivine (Fig. 4, B and C, and data S3). The bead analyzed here gives the most olivine-rich composition (~30% olivine), but all spherules define mineral proportions that imply an olivine websterite source (Fig. 4C).

The predicted compositions of minerals also exhibit a limited variation over the modeled *P-T* range (Fig. 4, D and E, and data S3). Both low-Ca and high-Ca pyroxenes in the modeled precursor of the bead analyzed here are more enstatite rich than pyroxenes in basalt 12005 and, to a lesser degree, lherzolite sample 67767 (Fig. 4D) (*31–33, 38*). The predicted composition of olivine in the target is also more Mg rich (Fo_{80}) than in the mare basalt ($Fo_{57–67}$) and lherzolite ($Fo_{67–73}$) (Fig. 4E), whereas plagioclase is more anorthite rich (*31–33, 38*), emphasizing the differences between these rocks and the precursor of the high-MgO glass beads.
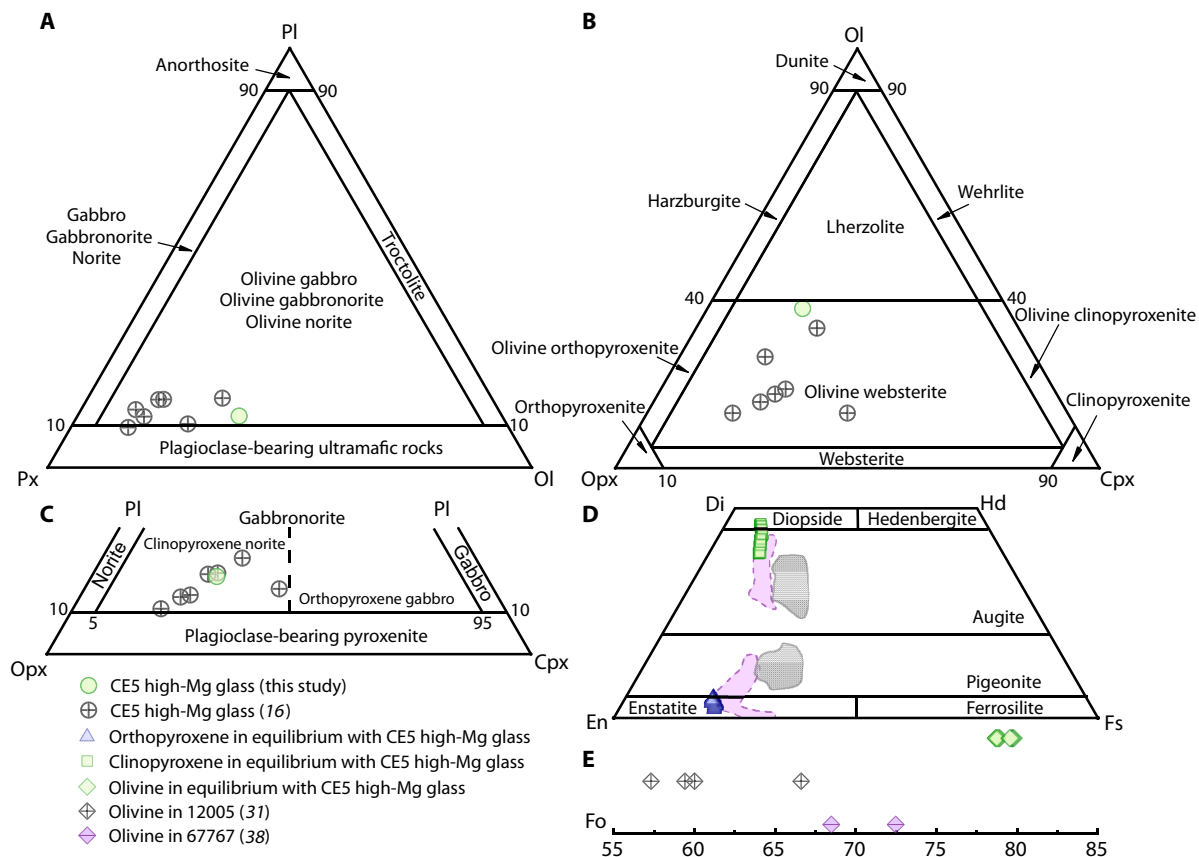

Fig. 4. Model mineral components and composition of the equilibrium phases corresponding to the composition of Chang'e-5 high-MgO glasses. (**A** to **C**) Average modal compositions of possible precursor rocks fall near the boundary between plagioclase-bearing ultramafic rocks and olivine-gabbro norites (clinopyroxene norite) and in the field of olivine websterites on the orthopyroxene-clinopyroxene-olivine diagram. (**D** and **E**) Comparison of pyroxene and olivine compositions in equilibrium phases in high-MgO beads and samples 12005 and 67767. The compositional ranges of pyroxene in 67767 and 12005 are shown in purple and gray, respectively. The published data in all plots are from (*31–33, 38*).

Crystallization of Mg-suite melts, mare basalts, or impact melts forms cumulates that might explain the mineralogy and chemistry of the high-MgO glass beads, in particular, their moderate enrichment in incompatible elements and the predicted presence of 10 to 15% plagioclase in their target rocks. Conversely, this mineralogy and chemistry contrast with the model compositions of mantle sources of mare basalts, which predict the presence of smaller (2 to 5 vol %) quantities of plagioclase and small amounts of trapped residual melt enriched in incompatible elements (*39*). However, there may be regions of the mantle with a higher proportion of entrained plagioclase than those sampled by mare basalts. It is also likely that large impacts variably excavated crustal and mantle lithologies (*40*), which may explain the presence of 10 to 15% plagioclase and the apparent enrichment in incompatible elements. Alternatively, the estimated proportion of plagioclase in the target may indicate incomplete separation of plagioclase during lunar magma ocean crystallization, assimilation of lower crust into the upper mantle during overturn (*37*, *39*, *41*), or redistribution of crustal plagioclase by impacts. The observed enrichment in incompatible elements in the high-MgO beads could also indicate a contribution from the urKREEP reservoir to the beads' precursor (Fig. 2) (*35*, *42*, *43*).

Low Ni and Co concentrations observed in the beads indicate an absence of any significant contribution of mature regolith to their compositions (*44*). The Ni/Co ratios of ~1 are similar to those of primitive mare basalt magmas (*45*) and are also consistent with low meteoritic contamination during the bead-forming impacts. However, the low Ni and Co concentrations also contrast with the composition of the mantle inferred from primitive mare basalts and volcanic glass beads, which have Ni and Co contents an order of magnitude higher than those of the Chang'e-5 high-MgO beads (*45*), with the mantle source regions of these magmas having even higher concentrations. An assessment of the relationships between MgO and Ni and Co concentrations in lunar mare basalts, volcanic glasses, high-MgO beads from Chang'e-5, and "komatiitic" beads from Apollo 16 regolith breccia (*22*) suggests that fractional crystallization or melting processes could not explain the observed differences (Fig. 2G). Consequently, the high-Mg beads from Chang'e-5 and the "komatiitic" beads either represent parts of a heterogeneous mantle that underwent a greater degree of metal loss or they experienced additional metal loss during the bead-forming impact. Low Ni and Co contents could also reflect local metal-silicate immiscibility within the bead, although only a small number of sumicrometer-sized Fe-rich inclusions are visible in the high-MgO bead investigated here (Fig. 1).

Possible location of high-Mg spherule precursor rocks and implications for lunar interior

The predicted mineralogy of the high-MgO Chang'e-5 glass precursors implies target lithologies rich in low-Ca pyroxene and olivine. A previous study (*42*) identified 531 locations on the Moon where SELENE (Kaguya) hyperspectral data indicate spectra dominated by low-Ca pyroxene, more than half of which are located around the rim of Imbrium basin (*42*). Fifteen low-Ca pyroxene locations are concentrated at the rim of Sinus Iridum on Imbrium's northwestern margin. Several olivine-rich exposures also occur in this area (*46*, *47*). In addition, remote sensing observations identified significant concentrations of low-Ca pyroxene around the South Pole Aitken basin, with some linked to the South Pole Aitken basin impact melt (*48*, *49*), whereas multiple sites dominated by olivine-rich rocks are

situated around the Moscoviense, Crisium, and Humboldtianum basins (*35*, *46*), as well as smaller craters such as Copernicus (*50*).

Several proposed scenarios explain the occurrence of olivine- and low-Ca pyroxene–bearing ultramafic rocks near the rims of these basins including the following: (i) different depths of excavation, resulting in the juxtaposition of olivine and pyroxene lithologies from different layers of a stratified mantle; (ii) lateral compositional heterogeneity of the lunar mantle; (iii) differentiation of thick impact melt sheets (*42*); and (iv) cumulates of Mg-suite magmas (*42*).

If impacts into parts of the upper lunar mantle brought to the (near) surface by the Imbrium event form the high-MgO beads, compositions of the beads suggest that at least parts of the upper mantle are dominated by pyroxene, particularly low-Ca pyroxene (orthopyroxene and/or pigeonite), with olivine less abundant. This conclusion is consistent with geophysical data and numerical simulations of mantle overturn (*51*, *52*). Previous studies have suggested a chemically stratified mantle with orthopyroxene as a major component (*35*) and perhaps even the predominant mineral in the upper lunar mantle (*51*). This is consistent with forward simulation models investigating the petrogenesis of lunar troctolite (*52*) and computational phase equilibrium models (*36*). In contrast, modeling of lunar magma ocean crystallization produced olivine and low-Ca pyroxene in the lower mantle and a clinopyroxene-rich upper mantle (*36*, *39*), although subsequent mantle overturn could have brought deeper material closer to the surface. Regardless of the specific explanation, the high-MgO beads from the Chang'e-5 soil represent unusual target lithologies such as those exposed at or near the rim of Sinus Iridum (Fig. 5), where spectra from multiple locations indicate both low-Ca pyroxene and olivine (*42*, *46*, *47*).

MATERIALS AND METHODS
Sample preparation and scanning electron microscopy
CNSA provided Chang'e-5 regolith sample CE5C0600YJFM00501 under the procedures for requesting lunar samples (*53*). We hand-picked the glass beads from the sample, embedded them in epoxy mounts, polished these mounts, and used a Carl Zeiss-Supra55 field emission scanning electron microscope at Nanjing University to obtain high-resolution backscattered electron images for investigation of textural features of the glass beads. The analytical setup included a 15-kV acceleration voltage and a working distance of ~8.5 mm.

Electron probe microanalysis
A JEOL JXA-8230 electron probe used to obtain major element compositions of the glass beads is located at State Key Laboratory of Critical Earth Material Cycling and Mineral Deposits, Nanjing University. The analytical conditions (data S1-1) included a 10-μm spot with the beam current set to 10 nA and a 15-kV accelerating voltage. Quantitative analyses had the detection limits for most elements in the range of 0.01 to 0.03 wt % and involved use of synthetic glasses and natural minerals as standards, the matrix corrections using ZAF procedures, and further assessment of the quality of the analyses using glass standards VG-2 and A-99 (data S1-2).

SIMS trace element analyses
On the basis of the electron probe microanalysis results, we selected 27 glass beads for trace elements analysis (data S1-3) using CAMECA
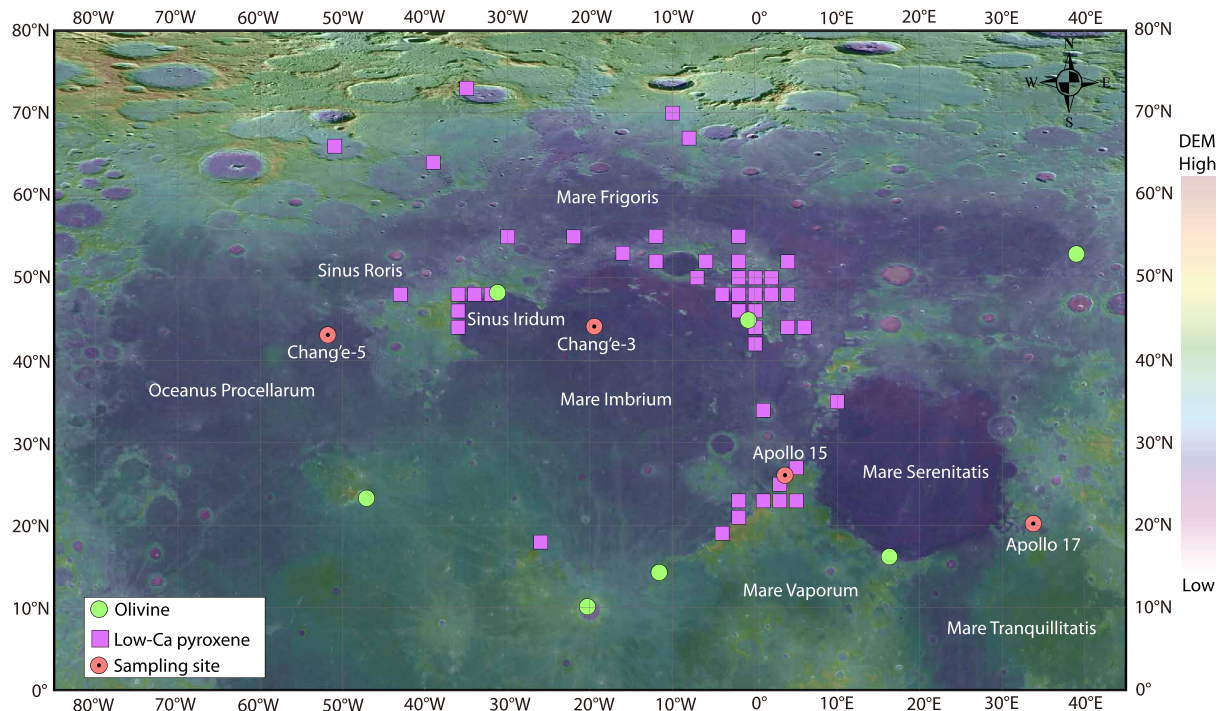
Fig. 5. Chang'e-1 CCD map showing possible regions of the origin of high-MgO glass beads. Different colors distinguish different geologic units on the digital elevation model (DEM) map of Chang'e-1. The locations of the low-calcium pyroxene and olivine outcrops concentrate around the rim of Imbrium basin (*42*, *46*). The Chang'e-1 global digital orthophoto model with a 120-m resolution and elevation model with a 500-m resolution dataset are available at https://dx.doi.org/10.12350/CLPDS.GRAS.CE1.DOM-120m.vA and https://dx.doi.org/10.12350/CLPDS.GRAS.CE1.DEM-500m.vA.

IMS-1300HR[3] SIMS at Nanjing University. Analysis of each spot included presputtering for 100 s using a 20 by 20–µm raster to remove the gold coating and minimize possible surface contamination. Analyses used a Gaussian illumination mode to focus a primary beam of $^{16}O_2^-$ with the intensity of around 10 nA. The final spot size was about 15 µm by 15 µm (with a 5-µm raster). To separate the light REE oxide interferences, the mass spectrometer setup included a mass resolution power of 15,000 (at 50% of peak height) with a 42-µm entrance slit and 82-µm exit slit. The analytical procedure involved detection of secondary ions in the monocollector mode and measuring the following mass sequence: ^{45}Sc, $^{30}Si^{16}O$, ^{51}V, ^{59}Co, ^{60}Ni, ^{89}Y, ^{90}Zr, ^{93}Nb, ^{139}La, ^{140}Ce, ^{141}Pr, ^{142}Nd, ^{147}Sm, ^{153}Eu, ^{158}Gd, ^{159}Tb, ^{163}Dy, ^{165}Ho, ^{167}Er, ^{169}Tm, ^{174}Yb, ^{175}Lu, ^{180}Hf, ^{181}Ta, ^{232}Th, and ^{238}U. Each spot analysis includes four cycles. We normalized intensities obtained for each isotope to $^{30}Si^{16}O$ and used the BHVO-2G glass standard (*54*) to obtain element concentrations of glass beads corrected for the matrix effects. The repeated measurements of BHVO-2G determined uncertainties of about ±1 to 4% for Sc, V, Co, Ni, Y, Zr, Nb, and light REE; ±2 to 7% for heavy REE, Th, and U; and ±10% for Ta. We used synthetic glass standards NIST-610 and NIST-612 to find peak positions for different elements and monitor the instrument stability and BCR-2G as a secondary standard to check the accuracy of the obtained trace element concentrations (*54*).

SIMS U–Pb analysis

The U and Pb isotope analyses in the glass beads conducted using CAMECA IMS-1300HR[3] SIMS at Nanjing University involved presputtering of each analytical spot for 80 s using a 20 by 20–µm raster before analysis to remove the gold coating and to minimize possible

surface contamination. The instrument setup included the following: (i) analysis in a Köhler illumination mode to focus a primary beam of $^{16}O_2^-$ with the intensity kept around 20 nA; (ii) the mass spectrometer operating at a mass resolution power of 8000 (50% peak height), with a 75-µm entrance slit and 175-µm exit slit to resolve Pb from molecular interferences; and (iii) secondary ions detection using multicollector with mass $^{204}Pb^+$ (L2), $^{206}Pb^+$ (L1), and $^{207}Pb^+$ (C) isotopes detected simultaneously, followed by stepping of the magnet field to analyze background, $^{238}U^+$ (L1), and $^{238}U^{16}O^+$ (L1) sequentially. Each analysis consisted of peak centering using $^{238}U^{16}O^+$, followed by measurements of U and Pb isotopes over 16 cycles with a total analytical time of 10 min. The optional instrument parameter, set up in the analysis recipe, helped to monitor backgrounds of electron multipliers.

The range of UO/O of lunar glass beads during SIMS analyses can be an order of magnitude larger than that of terrestrial glass standards (*8*), which can result in deviation of corrected Pb/U in the glass beads from the true values for up to 10 to 15% when using the conventional approach of plotting ln(Pb/U) versus ln(UO/U) for both standards and unknowns. To combat this problem, the calibration procedure used two terrestrial standard glasses BCR-2G (*54*) and T1-G (*55*) simultaneously. That allows to increase the range of UO/U in the standards and account for nonlinearity of ln(Pb/U) versus ln(UO/U) relationships that exists when UO/U shows an order of magnitude variation.

Phase equilibrium model

Phase equilibrium modeling involved use of the MAGEMin version 1.5.8 program that uses an internal thermodynamic dataset (*56*).

The modeling is based on the nine-component K_2O-Na_2O-CaO-FeO-MgO-Al_2O_3-SiO_2-TiO_2-Cr_2O_3 system. The thermodynamic solid solution and end-member database is based on the hydrous mafic melting model provided in (57). To accommodate for conditions relevant to the Moon, we set the temperature for model runs between 800° and 1700°C and the pressure between 0 and 4 kbar while keeping the oxygen content at 0.01 vol %, given the reducing conditions existing on the Moon. Data S3 provides the equilibrated compositions of different subphases.

Supplementary Materials

The PDF file includes:
Supplementary Text
Figs. S1 to S3
Legends for data S1 to S3
References

Other Supplementary Material for this manuscript includes the following:
Data S1 to S3

REFERENCES AND NOTES

1. A. M. Reid, J. Warner, W. I. Ridley, R. W. Brown, Major element composition of glasses in three Apollo 15 soils. *Meteoritics* **7**, 395–415 (1972).
2. A. M. Reid, W. I. Ridley, R. S. Harmon, J. Warner, R. Brett, P. Jakeš, R. W. Brown, Highly aluminous glasses in lunar soils and the nature of the lunar highlands. *Geochim. Cosmochim. Acta* **36**, 903–912 (1972).
3. A. M. Reid, J. Warner, I. Ridley, D. A. Johnston, R. S. Harmon, P. Jakes, R. W. Brown, The major element compositions of lunar rocks as inferred from glass compositions in the lunar soils. *Proc. Lunar Sci. Conf. 3rd* **1**, 363–378 (1972).
4. I. Ridley, A. M. Reid, J. Warner, R. W. Brown, R. Gooley, C. H. Donaldson, Glass compositions in Apollo 16 soils 60501 and 61221. *Proc. Lunar Sci. Conf. 4th* **4**, 309–321 (1973).
5. J. W. Delano, Pristine lunar glasses: Criteria, data, and implications. *J. Geophys. Res. Solid Earth* **91**, 201–213 (1986).
6. R. A. Zeigler, R. L. Korotev, B. L. Jolliff, L. A. Haskin, C. Floss, The geochemistry and provenance of Apollo 16 mafic glasses. *Geochim. Cosmochim. Acta* **70**, 6050–6067 (2006).
7. C. K. Shearer, J. J. Papike, Basaltic magmatism on the Moon: A perspective from volcanic picritic glass beads. *Geochim. Cosmochim. Acta* **57**, 4785–4812 (1993).
8. A. A. Nemchin, M. J. Whitehouse, M. L. Grange, J. R. Muhling, On the elusive isotopic composition of lunar Pb. *Geochim. Cosmochim. Acta* **75**, 2940–2964 (2011).
9. D. T. Wetzel, E. H. Hauri, A. E. Saal, M. J. Rutherford, Carbon content and degassing history of the lunar volcanic glasses. *Nat. Geosci.* **8**, 755–758 (2015).
10. A. E. Saal, E. H. Hauri, Large sulfur isotope fractionation in lunar volcanic glasses reveals the magmatic differentiation and degassing of the Moon. *Sci. Adv.* **7**, eabe4641 (2021).
11. W. Yang, Y. Chen, H. Wang, H.-C. Tian, H. Hui, Z. Xiao, S.-T. Wu, D. Zhang, Q. Zhou, H.-X. Ma, C. Zhang, S. Hu, Q.-L. Li, Y. Lin, X.-H. Li, F.-Y. Wu, Geochemistry of impact glasses in the Chang'e-5 regolith: Constraints on impact melting and the petrogenesis of local basalt. *Geochim. Cosmochim. Acta* **335**, 183–196 (2022).
12. A. E. Saal, E. H. Hauri, M. L. Cascio, J. A. Van Orman, M. C. Rutherford, R. F. Cooper, Volatile content of lunar volcanic glasses and the presence of water in the Moon's interior. *Nature* **454**, 192–195 (2008).
13. H. He, J. Yi, Y. Zhang, S. Hu, Y. Lin, H. Hui, J. Hao, R. Li, W. Yang, H. Tian, C. Zhang, M. Anand, R. Tartèse, L. Gu, J. Li, D. Zhang, Q. Mao, L. Jia, X. Li, Y. Chen, L. Zhang, H. Ni, S. Wu, H. Wang, Q. Li, H. He, X. Li, F. Wu, A solar wind-derived water reservoir on the Moon hosted by impact glass beads. *Nat. Geosci.* **16**, 294–300 (2023).
14. C. Zhou, B. Mo, H. Tang, Y. Gu, X. Li, D. Zhu, W. Yu, J. Liu, Multiple sources of water preserved in impact glasses from Chang'e-5 lunar soil. *Sci. Adv.* **10**, eadl2413 (2024).
15. T. S. Culler, T. A. Becker, R. A. Muller, P. R. Renne, Lunar impact history from $^{40}Ar/^{39}Ar$ dating of glass spherules. *Science* **287**, 1785–1788 (2000).
16. T. Long, Y. Qian, M. D. Norman, K. Miljkovic, C. Crow, J. W. Head, X. Che, R. Tartèse, N. Zellner, X. Yu, S. Xie, M. Whitehouse, K. H. Joy, C. R. Neal, J. F. Snape, G. Zhou, S. Liu, C. Yang, Z. Yang, C. Wang, L. Xiao, D. Liu, A. Nemchin, Constraining the formation and transport of lunar impact glasses using the ages and chemical compositions of Chang'e-5 glass beads. *Sci. Adv.* **8**, eabq2542 (2022).
17. A. A. Nemchin, M. D. Norman, M. L. Grange, R. A. Zeigler, M. J. Whitehouse, J. R. Muhling, R. Merle, U-Pb isotope systematics and impact ages recorded by a chemically diverse population of glasses from an Apollo 14 lunar soil. *Geochim. Cosmochim. Acta* **321**, 206–243 (2022).
18. N. E. B. Zellner, P. D. Spudis, J. W. Delano, D. C. B. Whittet, Impact glasses from the Apollo 14 landing site and implications for regional geology. *J. Geophys. Res. Planets* **107**, 5102 (2002).
19. R. L. Korotev, R. A. Zeigler, C. Floss, On the origin of impact glass in the Apollo 16 regolith. *Geochim. Cosmochim. Acta* **74**, 7362–7388 (2010).
20. K. Zong, Z. Wang, J. Li, Q. He, Y. Li, H. Becker, W. Zhang, Z. Hu, T. He, K. Cao, Z. She, X. Wu, L. Xiao, Y. Liu, Bulk compositions of the Chang'E-5 lunar soil: Insights into chemical homogeneity, exotic addition, and origin of landing site basalts. *Geochim. Cosmochim. Acta* **335**, 284–296 (2022).
21. W. F. McDonough, S.-s. Sun, The composition of the Earth. *Chem. Geol.* **120**, 223–253 (1995).
22. C. K. Shearer, J. J. Papike, K. C. Galbreath, S. J. Wentworth, N. Shimizu, A SIMS study of lunar "komatiitic glasses": Trace element characteristics and possible origin. *Geochim. Cosmochim. Acta* **54**, 1851–1857 (1990).
23. K. Mibe, T. Fujii, A. Yasuda, S. Ono, Mg–Fe partitioning between olivine and ultramafic melts at high pressures. *Geochim. Cosmochim. Acta* **70**, 757–766 (2006).
24. H. Hiesinger, R. Jaumann, G. Neukum, J. W. Head III, Ages of mare basalts on the lunar nearside. *J. Geophys. Res. Planets* **105**, 29239–29275 (2000).
25. B.-W. Wang, Q. W. L. Zhang, Y. Chen, W. Zhao, Y. Liu, G.-Q. Tang, H.-X. Ma, B. Su, H. Hui, J. W. Delano, F.-Y. Wu, X.-H. Li, Y. He, Q.-L. Li, Returned samples indicate volcanism on the Moon 120 million years ago. *Science* **385**, 1077–1080 (2024).
26. J. W. Head, L. Wilson, Y. Qian, Where on the Moon was the eruption that produced the recently reported ~ 120 million year old volcanic glass beads? *Icarus* **428**, 116378 (2025).
27. G. H. Heiken, D. S. McKay, R. W. Brown, Lunar deposits of possible pyroclastic origin. *Geochim. Cosmochim. Acta* **38**, 1703–1718 (1974).
28. M. J. Rutherford, J. W. Head, A. E. Saal, E. Hauri, L. Wilson, Model for the origin, ascent, and eruption of lunar picritic magmas. *Am. Mineral.* **102**, 2045–2053 (2017).
29. Z. Li, B. Zhang, S. Wang, X. Che, T. Long, Widespread involvement of low-abundance KREEP in the mantle of Chang'e-5 and its surrounding units. *Terra Nova* **37**, https://doi.org/10.1111/ter.12766 (2025).
30. J. J. Papike, G. Ryder, C. Shearer, "Lunar Samples" in *Planetary Materials* (The Mineralogical Society of America, 1998), pp. 5-001–5-234.
31. M. A. Dungan, R. W. Brown, The petrology of the Apollo 12 ilmenite basalt suite. *Proc. Lunar Sci. Conf. 8th* **8**, 1339–1381 (1977).
32. J. Rhodes, J. Brannon, K. Rodgers, D. Blanchard, M. Dungan, Chemistry of Apollo 12 mare basalts - Magma types and fractionation processes. *Proc. Lunar Sci. Conf. 8th* **8**, 1305–1338 (1977).
33. P. H. Warren, J. T. Wasson, The compositional-petrographic search for pristine nonmare rocks: Third foray. *Proc. Lunar Planet. Sci. Conf. 10th* **10**, 583–610 (1979).
34. K. Miljković, M. A. Wieczorek, G. S. Collins, S. C. Solomon, D. E. Smith, M. T. Zuber, Excavation of the lunar mantle by basin-forming impact events on the Moon. *Earth Planet. Sci. Lett.* **409**, 243–251 (2015).
35. D. P. Moriarty III, N. Dygert, S. N. Valencia, R. N. Watkins, N. E. Petro, The search for lunar mantle rocks exposed on the surface of the Moon. *Nat. Commun.* **12**, 4659 (2021).
36. T. E. Johnson, L. J. Morrissey, A. A. Nemchin, N. J. Gardiner, J. F. Snape, The phases of the Moon: Modelling crystallisation of the lunar magma ocean through equilibrium thermodynamics. *Earth Planet. Sci. Lett.* **556**, 116721 (2021).
37. L. T. Elkins-Tanton, S. Burgess, Q.-Z. Yin, The lunar magma ocean: Reconciling the solidification process with lunar petrology and geochronology. *Earth Planet. Sci. Lett.* **304**, 326–336 (2011).
38. E. C. Hansen, J. V. Smith, I. M. Steele, Petrology and mineral chemistry of 67667, a unique feldspathic lherzolite. *Proc. Lunar Planet. Sci. Conf. 11th* **11**, 523–533 (1980).
39. G. A. Snyder, L. A. Taylor, C. R. Neal, A chemical model for generating the sources of mare basalts: Combined equilibrium and fractional crystallization of the lunar magmasphere. *Geochim. Cosmochim. Acta* **56**, 3809–3823 (1992).
40. L. T. Elkins-Tanton, B. H. Hager, T. L. Grove, Magmatic effects of the lunar late heavy bombardment. *Earth Planet. Sci. Lett.* **222**, 17–27 (2004).
41. S. M. Elardo, D. S. Draper, C. K. Shearer Jr., Lunar Magma Ocean crystallization revisited: Bulk composition, early cumulate mineralogy, and the source regions of the highlands Mg-suite. *Geochim. Cosmochim. Acta* **75**, 3024–3045 (2011).
42. S. Yamamoto, H. Nagaoka, M. Ohtake, M. Kayama, Y. Karouji, Y. Ishihara, J. Haruyama, Lunar mantle composition based on spectral and geologic analysis of low-Ca pyroxene- and olivine-rich rocks exposed on the lunar surface. *J. Geophys. Res. Planets* **128**, e2023JE007817 (2023).
43. C. R. Neal, L. A. Taylor, Metasomatic products of the lunar magma ocean: The role of KREEP dissemination. *Geochim. Cosmochim. Acta* **53**, 529–541 (1989).
44. R. L. Korotev, The nature of the meteoritic components of Apollo 16 soil, as inferred from correlations of iron, cobalt, iridium, and gold with nickel. *J. Geophys. Res. Solid Earth* **92**, E447–E461 (1987).
45. J. M. D. Day, Metal grains in lunar rocks as indicators of igneous and impact processes. *Meteorit. Planet. Sci.* **55**, 1793–1807 (2020).

46. S. Yamamoto, R. Nakamura, T. Matsunaga, Y. Ogawa, Y. Ishihara, T. Morota, N. Hirata, M. Ohtake, T. Hiroi, Y. Yokota, J. Haruyama, Possible mantle origin of olivine around lunar impact basins detected by SELENE. *Nat. Geosci.* **3**, 533–536 (2010).

47. S. Yamamoto, M. Ohtake, Y. Karouji, M. Kayama, H. Nagaoka, Y. Ishihara, J. Haruyama, Global distribution and geological context of co-existing occurrences of olivine-rich and plagioclase-rich materials on the lunar surface. *J. Geophys. Res. Planets* **127**, e2021JE007077 (2022).

48. D. P. Moriarty III, C. M. Pieters, The character of South Pole-Aitken basin: Patterns of surface and subsurface composition. *J. Geophys. Res. Planets* **123**, 729–747 (2018).

49. C. Li, D. Liu, B. Liu, X. Ren, J. Liu, Z. He, W. Zuo, X. Zeng, R. Xu, X. Tan, X. Zhang, W. Chen, R. Shu, W. Wen, Y. Su, H. Zhang, Z. Ouyang, Chang'E-4 initial spectroscopic identification of lunar far-side mantle-derived materials. *Nature* **569**, 378–382 (2019).

50. D. Dhingra, C. M. Pieters, J. W. Head, Multiple origins for olivine at Copernicus crater. *Earth Planet. Sci. Lett.* **420**, 95–101 (2015).

51. O. L. Kuskov, E. V. Kronrod, V. A. Kronrod, Thermo-chemical constraints on the lunar bulk composition and the structure of a three-layer mantle. *Phys. Earth Planet. Inter.* **286**, 1–12 (2019).

52. T. C. Prissel, J. Gross, On the petrogenesis of lunar troctolites: New insights into cumulate mantle overturn & mantle exposures in impact basins. *Earth Planet. Sci. Lett.* **551**, 116531 (2020).

53. China National Space Administration (CNSA), "Notice of China National Space Administration on the distribution of procedures for requesting lunar samples (in Chinese and English)" (2020); www.cnsa.gov.cn/n6758823/n6758839/c6811124/content.html.

54. K. P. Jochum, U. Nohl, K. Herwig, E. Lammel, B. Stoll, A. W. Hofmann, GeoReM: A new geochemical database for reference materials and isotopic standards. *Geostand. Geoanalytical Res.* **29**, 333–338 (2005).

55. K. P. Jochum, B. Stoll, K. Herwig, M. Willbold, A. W. Hofmann, M. Amini, S. Aarburg, W. Abouchami, E. Hellebrand, B. Mocek, I. Raczek, A. Stracke, O. Alard, C. Bouman, S. Becker, M. Dücking, H. Brätz, R. Klemd, D. de Bruin, D. Canil, D. Cornell, C.-J. de Hoog, C. Dalpé, L. Danyushevsky, A. Eisenhauer, Y. Gao, J. E. Snow, N. Groschopf, D. Günther, C. Latkoczy, M. Guillong, E. H. Hauri, H. E. Höfer, Y. Lahaye, K. Horz, D. E. Jacob, S. A. Kasemann, A. J. R. Kent, T. Ludwig, T. Zack, P. R. D. Mason, A. Meixner, M. Rosner, K. Misawa, B. P. Nash, J. Pfänder, W. R. Premo, W. D. Sun, M. Tiepolo, R. Vannucci, T. Vennemann, D. Wayne, J. D. Woodhead, MPI-DING reference glasses for in situ microanalysis: New reference values for element concentrations and isotope ratios. *Geochem. Geophys. Geosyst.* **7**, Q02008 (2006).

56. N. Riel, B. J. P. Kaus, E. C. R. Green, N. Berlie, MAGEMin, an efficient Gibbs energy minimizer: Application to igneous systems. *Geochem. Geophys. Geosyst.* **23**, e2022GC010427 (2022).

57. T. J. B. Holland, E. C. R. Green, R. Powell, Melting of peridotites through to granites: A simple thermodynamic model in the system KNCFMASHTOCr. *J. Petrol.* **59**, 881–900 (2018).

58. M. D. Norman, K. J. D. Adena, A. G. Christy, Provenance and Pb isotopic ages of lunar volcanic and impact glasses from the Apollo 17 landing site. *Aust. J. Earth Sci.* **59**, 291–306 (2012).

59. T. P. Ding, H. G. Thode, C. E. Rees, Sulphur content and sulphur isotope composition of orange and black glasses in Apollo 17 drive tube 74002/1. *Geochim. Cosmochim. Acta* **47**, 491–496 (1983).

60. F. M. McCubbin, K. E. Vander Kaaden, R. Tartèse, R. L. Klima, Y. Liu, J. Mortimer, J. J. Barnes, C. K. Shearer, A. H. Treiman, D. J. Lawrence, S. M. Elardo, D. M. Hurley, J. W. Boyce, M. Anand, Magmatic volatiles (H, C, N, F, S, Cl) in the lunar mantle, crust, and regolith: Abundances, distributions, processes, and reservoirs. *Am. Mineral.* **100**, 1668–1707 (2015).

61. B. A. Wing, J. Farquhar, Sulfur isotope homogeneity of lunar mare basalts. *Geochim. Cosmochim. Acta* **170**, 266–280 (2015).

62. C. Petrowski, J. F. Kerridge, I. R. Kaplan, Light element geochemistry of the Apollo 17 site. *Proc. Lunar Sci. Conf. 5th* **5**, 1939–1948 (1974).

63. J. F. Kerridge, I. R. Kaplan, C. Petrowski, S. Chang, Light element geochemistry of the Apollo 16 site. *Geochim. Cosmochim. Acta* **39**, 137–162 (1975).